

Is it the boundaries or disorder that dominates electron transport in semiconductor ‘billiards’?

A.P. Micolich¹ *, A.M. See¹, B.C. Scannell², C.A. Marlow², T.P. Martin^{1,2} **, I. Pilgrim², A.R. Hamilton¹, H. Linke³, and R.P. Taylor²

¹ School of Physics, The University of New South Wales, Sydney NSW 2052, Australia

² Materials Science Institute, Physics Department, University of Oregon, Eugene OR 97403-1274, U.S.A.

³ Solid State Physics and nmC@LU, Lund University, Box 118, SE-221 00, Lund, Sweden

Key words quantum chaos, semiconductor billiards, quantum dots, ballistic transport

Semiconductor billiards are often considered as ideal systems for studying dynamical chaos in the quantum mechanical limit. In the traditional picture, once the electron’s mean free path, as determined by the mobility, becomes larger than the device, disorder is negligible and electron trajectories are shaped by specular reflection from the billiard walls alone. Experimental insight into the electron dynamics is normally obtained by magnetoconductance measurements. A number of recent experimental studies have shown these measurements to be largely independent of the billiards exact shape, and highly dependent on sample-to-sample variations in disorder. In this paper, we discuss these more recent findings within the full historical context of work on semiconductor billiards, and offer strong evidence that small-angle scattering at the sub-100 nm length-scale dominates transport in these devices, with important implications for the role these devices can play for experimental tests of ideas in quantum chaos.

Copyright line will be provided by the publisher

Contents

1	Introduction	1
2	Semiconductor quantum dots - The fundamentals	2
2.1	Making quantum dots	2
2.2	Length scales and transport regimes	3
2.3	Quantum interference and conductance fluctuations	4
3	Early pictures of quantum chaos in semiconductor billiards	5
4	The trouble with semiconductor billiards - Soft walls and small-angle scattering	7
4.1	Soft-walls and mixed phase-spaces	7
4.2	Remote ionized dopants and small-angle scattering	9
5	Discussion	11
6	Acknowledgements	13
	References	13

1 Introduction

Quantum mechanics and chaos theory are two great discoveries of the 20th century. Combining them leads to highly interesting and important questions; for example, how does the uncertainty principle’s inherent ‘blurriness’ affect the sensitivity to initial conditions characteristic of chaotic systems? Quantum chaos rose to popular attention in the 1970s, first in the context of electron dynamics in atoms [1, 2],

* Corresponding author E-mail: adam.micolich@nanoelectronics.physics.unsw.edu.au

** Current address: Acoustics Division, Naval Research Laboratory, Washington, DC 20375, U.S.A.

and subsequently for model two-dimensional (2D) dynamical systems known as ‘billiards’ [3, 4]. From a classical perspective, a billiard contains a particle traveling in straight lines between specular reflections at a shaped boundary wall. A variety of billiard shapes have been studied ranging from simple geometries (e.g., circle or square) to more complex geometries (e.g., stadia and ‘lemon’ billiards [5]) and geometries with multiple topologically-independent walls (e.g., the Sinai billiard [6]). Billiards have since become an archetypal system for studies of quantum chaos [7, 8].

The quest for experimental realizations of quantum billiards naturally followed, with microwave billiards formed in open resonators [9–11] and superconducting slabs [12] leading the way, closely followed by semiconductor microstructures [13–15]. In the years that followed, quantum billiards have also been realized in quantum ‘corrals’ defined by scanning tunneling microscopy on metal surfaces [16, 17], in acoustic systems [18, 19], atom-optics systems [20, 21], and various optical systems including micro-cavity lasers [22] and double-clad optical fibers [23, 24].

An important consideration in comparing measurements to theoretical expectations is to adequately account for practical aspects of the experimental implementation that affect the correspondence. For semiconductor billiards, two important aspects are the electrostatic nature of confinement and impurities in the semiconductor [25]. These aspects, impurity scattering in particular, were considered in initial studies [13, 14, 26, 27] and suggested to not obscure the essential physics. This has resulted in a widely-held perception that semiconductor microstructures are an ideal test-bed for dynamical quantum chaos; for example, “... it is important to understand the consequences of non-diffusive electron dynamics on the electronic conductance or other transport properties. This question has been studied in much detail for semiconductor nanostructures in which the motion of electrons is ballistic rather than diffusive. In such systems, disorder is negligible, and, consequently, all transport properties are determined by the shape of the sample, as in a billiard model.” [28]. However, a range of experiments following these initial studies have gradually shown that impurity scattering not only cannot be ignored, but may actually dominate over boundary-dependent ‘ballistic’ transport in semiconductor billiards.

Here, we provide a short, focussed review of studies of electron transport in semiconductor microstructures, and offer evidence that these devices are not the ideal embodiment of quantum dynamical billiards, as is often thought based on the pioneering papers on this topic [13, 14, 29–31]. Our aim is to show that the true picture of transport in these devices is much more complex than initially anticipated.

2 Semiconductor quantum dots - The fundamentals

2.1 Making quantum dots

The underpinning structure for most studies of semiconductor quantum dots and billiards is the modulation-doped AlGaAs/GaAs heterostructure [32]. It typically consists of a GaAs substrate supporting an undoped AlGaAs spacer layer, a Si-doped AlGaAs modulation-doping layer, and an undoped GaAs cap layer (Fig. 1(b)) grown using molecular beam epitaxy (MBE) [33]. The narrow, triangular potential well at the AlGaAs/GaAs interface forms self-consistently through the band-bending induced by ionization of the Si dopants (Fig. 1(c)). The well width is comparable to the electron Fermi wavelength ($\lambda_F \sim 50$ nm), strongly confining the electrons in the growth direction to form a two-dimensional electron gas (2DEG). Further confinement of the 2DEG is typically achieved using a set of metal surface electrodes (gates) defined using electron beam lithography techniques [34, 35] (Fig. 1(a)). Application of a negative bias V_g to the gates electrostatically depletes the 2DEG directly underneath, transferring the gate pattern into the 2DEG as shown in Fig. 1(b).¹ The result is a quasi-zero-dimensional quantum dot connected by small one-dimensional (1D) entrance and exit ports to 2DEG source and drain reservoirs. These are connected to the external circuit via diffused AuGeNi ohmic contacts.

¹ A common alternative is to selectively etch away the doping, which also gives patterned depletion regions in the 2DEG.

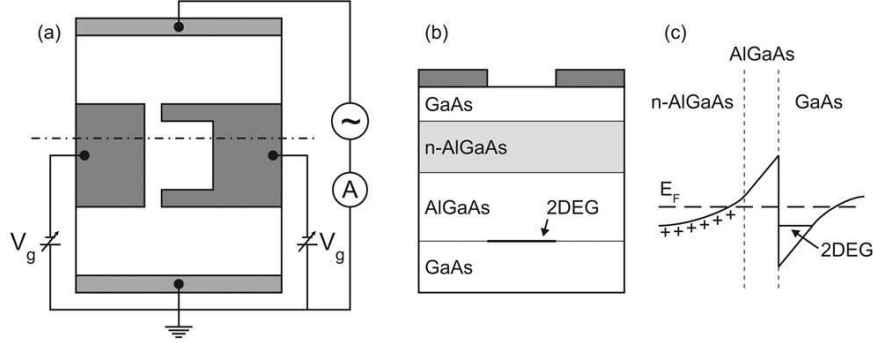


Fig. 1 (a) Top view of a semiconductor billiard including basic measurement circuit. The billiard is defined by a pair of metal surface electrodes (gates) with a negative d.c. bias V_g applied, and connected to the measurement circuit via 2DEG source and drain reservoirs, each featuring an AuGeNi ohmic contact. The dot-dashed line indicates the cross-section presented in (b). (b) heterostructure cross-section illustrating electrostatic depletion due to the negatively-biased gates. (c) Conduction band diagram illustrating 2DEG formation at the AlGaAs/GaAs interface. The dashed line indicates the electron Fermi energy E_F and + the ionized Si dopants in the n-AlGaAs layer.

2.2 Length scales and transport regimes

A hallmark of MBE-grown AlGaAs/GaAs heterostructures is an extremely high electrical mobility, typically $\mu \sim 10^5 - 10^7$ cm²/Vs, corresponding to an electron mean free path $\ell \sim 0.5 - 50$ μ m at a typical 2DEG electron density $n \sim 10^{11}$ cm⁻². The traditional paradigm of transport regimes in mesoscopic devices [36] depends on the relationship between ℓ and the device's length L and width W (Fig. 2(a-c)). In the diffusive regime, $\ell < L, W$, the electron's trajectory is primarily determined by the impurity configuration (Fig. 2(a)). In the ballistic regime, $\ell > L, W$, there are no impurities within the device on average, and an electron follows straight line paths between specular reflections at the device boundary (Fig. 2(c)). In the quasi-ballistic regime, $\ell \sim L, W$ or $W < \ell < L$, a mixture of impurity and boundary scattering determines the electron's trajectory (Fig. 2(b)). The quantum dots used as billiards typically have $L, W < 1$ μ m and $\ell > 2$ μ m.

For later discussion, it is worth bearing in mind that this is a somewhat simplistic and incomplete picture of disorder in these devices, because μ is heavily weighted towards large-angle scattering events [37]. As a result, small-angle scattering is often under-appreciated; we will return to this in §4.2.

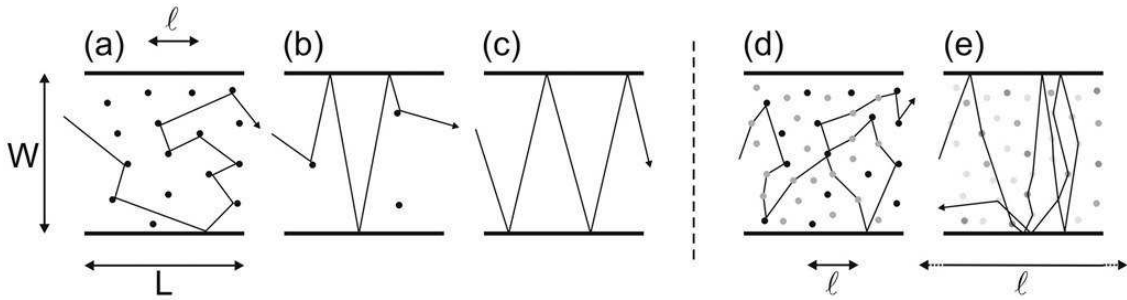


Fig. 2 (a-c) The traditional paradigm of transport regimes in mesoscopic devices [36]: (a) diffusive $\ell < L, W$, (b) quasi-ballistic $\ell \sim L, W$, and (c) ballistic $\ell > L, W$. L and W are the device/channel length and width and ℓ is the electron mean free path determined from the electrical mobility μ . (d/e) Schematics for a modified picture of the (d) diffusive and (e) ballistic regimes accounting for small-angle ionized impurity scattering, as discussed in §4.2. The lighter dots in (d/e) correspond to small-angle scatterers, with darker shades representing a greater propensity towards larger scattering angles.

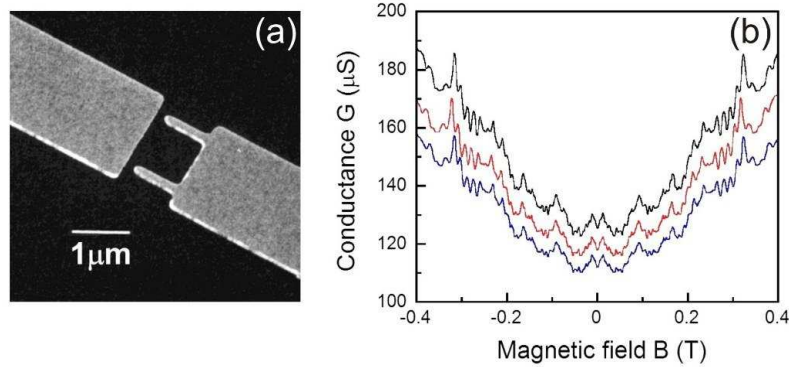


Fig. 3 (a) Scanning electron micrograph of a typical quantum dot device with Ti/Au gates (grey) on the GaAs surface (black). The $1 \times 1 \mu\text{m}$ quantum dot is connected to 2DEG source and drain reservoirs via 1D quantum point contact (QPC) entrance and exit ports. (b) Conductance G versus magnetic field B perpendicular to the 2DEG from the device in (a). Three traces are shown; the upper and middle traces are subsequent sweeps of B , the lower trace was obtained 10 hours later, on returning the device to the same V_g used for the first two traces after other measurements.

2.3 Quantum interference and conductance fluctuations

The Aharonov-Bohm (AB) effect [38] demonstrates the influence of electromagnetic potentials on quantum interference. The original concept involved an infinite length solenoid, with an electron beam split and recombined in the plane perpendicular to the solenoid axis to form an interferometer ‘loop’. For an infinitely long solenoid, the field B experienced by the electrons is zero; the AB effect is caused by the magnetic vector potential \mathbf{A} , such that electrons traversing opposite arms of the loop accumulate phase terms of opposing sign $\pm(e/\hbar) \int \mathbf{A} \cdot d\mathbf{l}$, where $d\mathbf{l}$ is an element of path length. The two electron beams interfere when recombined, giving a transmitted beam intensity that is an oscillatory function of the flux ϕ enclosed by the loop (and in this case, restricted entirely to the solenoid’s interior). Early electron microscope experiments demonstrated flux-induced electron interference [39], but it took another 25 years to demonstrate interference occurring via the vector potential \mathbf{A} alone [40].²

The Aharonov-Bohm effect lays at the heart of a range of magnetic field induced fluctuations in the electrical conductance of mesoscopic devices. At its simplest, it produces a sinusoidal fluctuation with a period $\Delta B = h/eA$ in the conductance G of nanoscale ring structures enclosing an area A ; observed in both gold rings [41] and etched ring-shaped structures in an AlGaAs/GaAs heterostructure [42]. These experiments are performed at a temperature $T < 1$ K using a ^3He cryostat or a $^3\text{He}/^4\text{He}$ dilution refrigerator to ensure electron phase coherence. The conductance fluctuations develop richer structure when the interference involves a larger number of possible electron paths through the device. A classic example is the $1 \mu\text{m}$ square quantum dot in Fig. 3(a), which is connected to 2DEG source and drain reservoirs via a pair of Quantum Point Contact (QPC) entrance and exit ports. The QPC strongly diffracts the incoming electron wave [43, 44], allowing a range of trajectories linking the entrance and exit QPCs to interfere and contribute to G . In a semiclassical picture, each trajectory pair encloses a different area θ , giving a slightly different period of AB oscillation; these combine to yield reproducible multi-spectral magnetoconductance $G(B)$ fluctuations (Fig. 3(b)). These fluctuations are not noise; as the lower trace in Fig. 3(b) demonstrates, identical fluctuations are obtained if a device returned to a given gate bias configuration after measurements at other biases, providing the temperature remains low throughout (see §4.2). The link between the spectral content of the magnetoconductance fluctuations (MCF) and the distribution of loop areas $N(\theta)$ [45] provides a ‘magnetofingerprint’ of the electron trajectories within the dot [46, 47]. While the underlying mechanism for these fluctuations is the same as that driving the well-known Universal Conductance Fluctuations (UCF) [47–53], the amplitude of the fluctuations for dots is not universal [13]; this is due to the lack

² Superconducting films were used to screen the electron beams from any magnetic field B generated whilst establishing \mathbf{A} .

of ensemble averaging that occurs in diffusive systems [48, 49, 52, 53]. Another commonly held difference between UCF in metals or MOSFETs and MCF in quantum dots is that whereas in the former transport is diffusive, in the latter the transport is assumed to be ballistic and hence determined by the geometry of the dot walls. We will return to examine this assumption in §4.2 in light of recent experiments [54, 55] that question the way we think about semiconductor billiards as systems for studying quantum chaos.

3 Early pictures of quantum chaos in semiconductor billiards

The use of ballistic microstructures for studies of quantum chaos [56] evolved from experimental studies of ballistic junction devices [57, 58] in the late 1980s. In particular, a seminal theoretical paper by Jalabert *et al* [29] proposed that knowledge of the chaotic classical scattering dynamics could be used to predict quantitatively measurable properties of ballistic microstructures. This relies on a universal property of chaotic dynamics in open scattering systems whereby a particle's probability of escape is exponential in time [59], giving measurable correlations in the energy/frequency spectrum [60, 61]. Jalabert *et al* extended this property to ballistic microstructures, translating the escape time distribution into a distribution of accumulated trajectory areas, which, using semiclassical arguments, produces MCF with particular statistical properties via the AB effect. In particular, the autocorrelation function $C(\Delta B) = \langle \delta g(B) \delta g(B + \Delta B) \rangle$ for the MCF should take the form:

$$C(\Delta B) = C(0)/[1 + (\Delta B/\alpha\phi_0)^2]^2 \quad (1)$$

where $\delta g(B)$ is the fluctuation from mean conductance. Here $\phi_0 = h/e$ and α is the exponent for the distribution $N(\theta) \propto \exp(-2\pi\alpha|\theta|)$ of areas θ enclosed by various possible trajectories [13, 29].

Marcus *et al* [13] reported the first experiment devoted specifically to chaotic scattering in ballistic microstructures, measuring two separate chips, each containing two quantum dots, one with a circular geometry and one with a stadium shaped geometry. The study had two intentions: to confirm the prediction by Jalabert *et al* [29] for chaotic scattering systems, and to confirm predictions of quantitative statistical differences in the fluctuations between geometries supporting chaotic (stadium) and non-chaotic (circle) transport [62, 63]. Comparison with theoretical expectations in Ref. [29] was made via the Fourier transform of Eq. 1, which gives the MCF power spectrum [13]:

$$S(f) = S(0)[1 + (2\pi\alpha\phi_0)f]e^{-2\pi\alpha\phi_0 f} \quad (2)$$

Fits of Eq. 2 for the stadium geometry gave $\alpha\phi_0 \sim 3.6$ mT, corresponding to an $\alpha^{-1} \sim 2.7$ times the dot area A , consistent with expectations from Ref. [29]. The spectral power $S(f)$ for the circle was similar at $f < 250 \text{ T}^{-1}$ but higher at $250 < f < 1000 \text{ T}^{-1}$, consistent with predictions of enhanced higher frequency content, corresponding to a larger number of large-area trajectories in non-chaotic geometries [62, 63]. Note that the power spectra used for comparison to Ref. [29] were heavily averaged (15 fast Fourier transform (FFT) spectra from half-overlapping 256-point (18.6 mT) wide windows). Single FFT spectra for 1024 point blocks spanning $-70 < B < 70$ mT revealed structure at low frequencies, consistent with structure in the large ΔB tails of the $C(\Delta B)$ versus ΔB data presented in Ref. [13]. Such low frequency spectral peaks are an expected signature of wavefunction scarring by periodic orbits [4, 44, 64], and have been extensively studied in subsequent calculations [43, 44, 65], transport studies [66] and scanning-gate microscopy (SGM) studies [67–69]. However, of particular note for the discussion in §4.2 is a comparison between the power spectra for nominally identical geometries (i.e., the stadium on device 1 with the stadium on device 2 or the circle on device 1 with the circle on device 2) in Fig. 3 of Ref. [13]. If the dominant factor in determining the trajectory distribution is device geometry, then the spectra for identical geometries on different chips should match, or at least be very similar; they instead differ significantly, indicating that dot shape alone cannot account for the electron dynamics.

Subsequent theoretical work by Baranger *et al* [30] proposed the alternative possibility of distinguishing between geometries supporting chaotic and regular (i.e., non-chaotic) dynamics using the ‘ballistic’ analog [13] of another important interference effect in diffusive 2D systems known as weak localization (WL) [70]. Weak localization involves interference between a trajectory that returns to its point of origin via a set of impurity scattering events, and its time-reversed counterpart. Application of an increasing perpendicular magnetic field B progressively breaks time-reversal symmetry for shorter length paths, leading to a positive magnetoconductivity correction (minima in $G(B)$ at $B = 0$), and hence a peak in the magnetoresistance.³ The proposal by Baranger *et al* [30] is that the different dynamics produce different WL peak lineshapes, which relies on the distribution of enclosed loop areas $N(\theta)$ differing between chaotic and regular billiards. Under a semiclassical framework, the average quantum correction to the reflection coefficient R_D for chaotic billiards takes the form:

$$\langle \delta R_D(B) \rangle = R/[1 + (2B/\alpha\phi_0)^2] \quad (3)$$

where $R = \langle \delta R_D(B = 0) \rangle$ [74], and for regular billiards:

$$\langle \delta R_D(B) \rangle \propto |B| \quad (4)$$

for small B [30]. It is important that the average above is taken over an infinite window in k to ensure that the contributions to Eq. 3/4 only include the interference of paths that are precise time-reversed pairs. This averaging has important experimental implications – the geometry effect should not be directly observable in a single magnetoresistance $R(B)$ trace, but only when sufficient averaging is applied to eliminate the conductance fluctuations [74]. Indeed, it is reported in Ref. [74] that calculations of unaveraged $R(B)$ traces yield a *minimum* at $B = 0$ in $\sim 33\%$ of cases, in contrast to the expected $B = 0$ maxima. This is borne out experimentally; e.g., in studies of dots featuring an additional ‘shape-distorting’ gate by Chan *et al* [75] averaging was needed to obtain a clear Lorentzian $R(B)$ peak and $R(B)$ minima are occasionally observed [76], in studies of a square billiard by Bird *et al* [77] where $R(B)$ peak lineshape (Lorentzian vs linear) was sensitive to gate voltage, and in studies by Keller *et al* [78] where $G(B)$ maxima and minima were obtained at different densities (i.e., Fermi energy) while the ensemble-average $\langle G(B) \rangle$ gave the expected minima at $B = 0$.

Measurements by Chang *et al* [14] provided evidence in support of the prediction by Baranger *et al* above; reporting a Lorentzian $R(B = 0)$ peak for a stadium geometry (chaotic) and a linear $R(B = 0)$ peak for a circular geometry (non-chaotic). It is very important to note that these studies were not performed in single dots, but in devices consisting of 48 dots with nominally-identical geometry arranged in a 6×8 array. This is vital in terms of the averaging issues discussed in Ref. [74], but may also have important implications in terms of small-angle scattering, as we will discuss in §5.

This brings us to an important turning point in terms of our understanding of ballistic transport and quantum chaos in semiconductor billiards and quantum dots. On the basis of the work discussed above it is tantalizing and easy to assume a great simplicity in these devices: images of electrons traveling along straight line trajectories between specular reflections from walls with well defined geometrical shapes, clear divisions of geometries into chaotic and non-chaotic, which in turn give clear and distinct experimental signatures, etc. see, e.g., Ref. [31]. As the following discussion will show, in reality, the picture of electron dynamics in semiconductor billiards is more complex. The practicalities involved in the experimental realizations have effects that are far from negligible, and that will ultimately force us to rethink our understanding of the results previously described in this section.

³ n.b. alternative explanations for the magnetoconductivity about $B = 0$ in quantum dots have also been subsequently proposed [71–73].

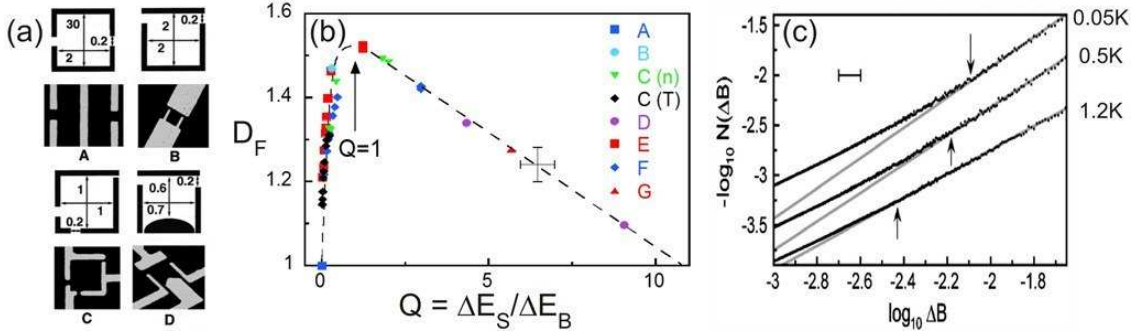


Fig. 4 (a) Gate schematics (top) and scanning electron micrographs (bottom) for the seven billiard devices studied in Ref. [85]. Devices E, F and G are identical to B with widths of 1, 0.6 and 0.4 μm , respectively. The digits in (a) indicate lengths/widths in μm ; Ti/Au gates appear grey on the GaAs surface (black). (b) Measured fractal dimension D_F versus Q , which quantifies the resolution of quantized energy levels within the billiard [85]. (c) Fractal scaling plot for $G(B)$ data from the ‘disrupted’ billiard from Ref. [89] at $T = 50$ mK (top), 500 mK and 1.2 K (bottom). The arrows indicate the lower cutoff for fractal scaling.

4 The trouble with semiconductor billiards - Soft walls and small-angle scattering

4.1 Soft-walls and mixed phase-spaces

The complexities involved in the theoretical calculations described above typically forced semiconductor billiards to be stripped down to their most basic elements for modeling (particularly in the early 90s, where computational capabilities were not what they are today). The early models of dynamics in semiconductor microstructures assumed hard-walls (i.e., the location of the wall in terms of particle reflection is independent of energy) and geometries where the phase space is either completely chaotic (ergodic) or completely regular. However, semiconductor billiards are defined by electrostatic depletion of selected regions of the 2DEG, using either negatively biased surface-gates or by locally etching away the dopants. This naturally results in a soft-wall potential [79, 80], often best approximated as parabolic [25]. This profile results generically in a mixed phase-space, containing both chaotic and regular regions; the ramifications of this were explored by Ketzmerick [81]. Trapping by the infinite hierarchy of Cantori at the boundaries between regular and chaotic regions in the phase space causes the escape time probability distribution to take a power-law form $P(t) \sim t^{-\beta}$ with exponent $\beta \leq 2$. This was expected via semiclassical arguments to produce a power-law distribution of enclosed areas $N(\theta) \sim \theta^{-\gamma}$ for large θ and statistically self-similar fractal conductance fluctuations with fractal dimension $D_F = 2 - \gamma/2$ for $\gamma \leq 2$ (and $D_F = 1$ for $\gamma > 2$) [81].

The observation of statistically self-similar fractal conductance fluctuations in billiards was independently reported first by Micolich *et al* [82] and soon thereafter by Sachrajda *et al* [83].⁴ In both cases, fractal dimensions $1 < D_F < 2$ were reported, with preliminary analyses reporting dependencies of D_F on external parameters such as gate voltage and temperature [82, 83].

A subsequent, more extensive study of the dependence of D_F on a range of parameters involving seven separate devices (Fig. 4(a)) by Micolich *et al* [85] lead to a remarkable finding: a plot of D_F versus a single parameter Q for many $G(B)$ traces all fall onto a single curve (Fig. 4(b)), despite being obtained from seven different sizes and shapes of device with differing number of 1D modes n passing through the

⁴ n.b., Exact self-similarity in a semiconductor Sinai billiard was reported by Taylor *et al* [84] a year prior.

QPC entrance and exit ports, electron mean free path ℓ and temperature T . The parameter Q is the ratio of the average energy level spacing ΔE_S to the average energy broadening ΔE_B for the dot, taking the form:

$$Q = \frac{\Delta E_S}{\Delta E_B} = \frac{2\pi\hbar^2}{m^*A} \frac{1}{\sqrt{(\hbar/\tau_q)^2 + (k_B T)^2}} \quad (5)$$

where m^* is the electron effective mass and τ_q is the lifetime of the quantum states, obtained using a skipping orbit analysis [86–88].⁵ Remarkably, D_F is found to take its maximum value ~ 1.52 at $Q = 1$, with D_F falling in either direction, reaching the non-fractal value $D_F = 1$ in the limits $Q = 0$ and $Q \sim 10$. The trend in the small Q limit is particularly interesting; small Q is typically achieved via the denominator through increases in T and/or decreases in τ_q . Based purely on Ref. [81], one would expect that a reduction in the coherence length (and thus τ_q) independent of other billiard parameters would reduce the scaling range over which fractal behaviour was observed but not alter D_F itself. Indeed, later work (Fig. 4(c)) showed that the scaling range instead increases with increasing temperature concurrent with a falling D_F [89]. Calculations by Budiyo and Nakamura [90] based on a semiclassical Kubo formalism obtained a D_F that decreases smoothly with increasing T ; an interesting side-aspect of these calculations is a connection to the Weierstrass function model [91, 92] for the exact self-similarity reported in Sinai billiards [84]. Hennig *et al* [93] provide an interesting alternative, suggesting that the underlying classical dynamics also lead to fractal conductance fluctuations. As such, $G(B)$ is a superposition of two fractals, one due to quantum interference, which is suppressed by decoherence to reveal fractal fluctuations due to the classical processes. Note that the data below the lower cut-off (i.e., low ΔB limit) in Fig. 4(c) is linear with a different slope. This might be indicative of a process similar to that proposed by Hennig *et al*, however, care is needed as this data is close to the resolution limit/noise floor; further experiments in this direction are warranted. Several studies suggest that the semiclassical theory proposed by Ketzmerick [81] is only part of a larger picture. A complete discussion is beyond the scope of this paper, but most significantly, mixed phase space does not appear essential to the generation of fractal conductance fluctuations [94, 95], which are also expected theoretically for completely chaotic [95–97] and completely integrable [98] billiards.

Considering Ketzmerick's theory, an interesting parameter to vary is the softness of the billiard walls. The first studies were performed by using a pair of billiards defined, one above the other, in a double quantum well heterostructure to provide identical geometries with different wall softness [99]. Self-consistent potential simulations [100] showed that the profile gradient at the Fermi energy differed by a factor of three between the 90 and 140 nm deep billiards [99]. The data in both billiards was consistent with Eq. 5; the only difference compared to the data in Fig. 4(b), which contains the shallower billiard data as device C, is that the deeper billiard (harder potential) gave a lower maximum $D_F \sim 1.45$ at $Q = 1$ [89]. This difference in maximum D_F is small, and may be due to competing effects given the complexities of this device [99].

The effect of soft-wall profile was also studied by Marlow *et al* [101]. A further 21 devices were investigated: 11 Ga_{0.25}In_{0.75}As/InP billiards and 5 Ga_{0.25}In_{0.75}As/InAlAs billiards of various geometries, and 5 GaAs quantum wires. As demonstrated by Martin *et al* [102], the potential profile for the etched GaInAs/InP billiards⁶ is ten times steeper than for the surface gated AlGaAs/GaAs billiards in Ref. [85, 89]. Despite this, the data for all of these devices closely overlays that in Fig. 4(b), suggesting that wall profile is not a determining factor for D_F . The data obtained for quasi-ballistic and diffusive GaAs quantum wires was also fractal and fit on the curve in Fig. 4(b). This is consistent with earlier work showing fractal conductance fluctuations in quasi-ballistic gold nanowires [103], and predictions that fractal conductance fluctuations survive diffusive transport [97].

⁵ This is ultimately an unentangleable combination of the phase coherence time τ_ϕ and the escape time related to a skipping orbit finding a QPC through which to exit the dot.

⁶ The substitution of InAlAs for InP should not affect the profile of the billiard walls. The slight change in band-gap (from ~ 1.42 eV to ~ 1.55 eV) should not significantly affect the 2DEG confinement either. There is a large difference in disorder however, as described in the text and Ref. [101].

Ultimately, the results obtained by Micolich *et al* [85, 89] and Marlow *et al* [101] suggest that the statistical properties of the conductance fluctuations, at least in terms of fractal dimension, are independent of the geometry of the billiard walls⁷. This is unexpected given that transport in these devices is nominally ‘ballistic’. Instead, the statistical properties via Eq. 5 and Q , depend only on A , T and τ_q irrespective of the specifics of the sample itself. This ‘universality’ bears a strong resemblance to that of Universal Conductance Fluctuations (UCF) in mesoscopic metal films and MOSFETs (see, for example, Fig. 3 of Skocpol [53]) where the transport is diffusive rather than ballistic. This raises interesting and radical questions: Even though $\ell \gg L, W$ for billiards and they are ballistic by traditional measures [36], is the transport really ballistic? Or is it diffusive, such that a form of scattering essentially undetected by the mobility, dominates the transport?

4.2 Remote ionized dopants and small-angle scattering

The 2DEG in an AlGaAs/GaAs heterostructure is normally populated by the ionization of remote Si dopants. These positively charged ionized dopants interact electrostatically with the electrons in the 2DEG causing significant scattering. High mobility 2DEGs are obtained through a process known as ‘modulation doping’ [32], where the Si dopants are separated from the 2DEG by a 20–100 nm undoped AlGaAs spacer layer. The key to modulation doping is that ionized dopants are converted from large-angle scattering sites to small-angle scattering sites by increases in the dopant-2DEG separation. This effectively ‘hides’ some of the ionized dopant scattering because the mobility is weighted towards large-angle scattering [37, 105] (see §5). Nonetheless, the 2DEG still feels the effect of the ionized dopants, which present as a low-level ($\sim 1 - 10$ meV) random ‘disorder potential’ for the electrons [106]. The length scale of this scattering is set by the 2DEG-donor separation [107], usually of order 20–100 nm, is much smaller than the typical billiard width ($\sim 0.6 - 2 \mu\text{m}$) and the large-angle scattering length $\ell \sim 2 - 20 \mu\text{m}$.

At the time of the initial studies [13, 14, 29, 30, 36], knowledge of the effect that the underlying disorder potential had on ballistic transport in microstructures was relatively low, although numerical simulations showed it could significantly affect transport at length scales much smaller than ℓ [108]. The first focussed consideration in terms of billiards was by Lin, Delos and Jensen [27], and involved adding a random angle $[-\pi, +\pi]$ at each wall reflection in a semiclassical dynamical model for stadium and circle billiards. The focus was on the statistics, and while the disorder in this model had little effect for the stadium (as expected given the ergodic dynamics), it destroyed the power-law tail in the area distribution for the circular billiard. This gave an exponential distribution, as expected for the stadium billiard, albeit with a different exponent [27]. This should produce a Lorentzian $R(B = 0)$ peak for both stadium and circle billiards. Chang *et al* [14] approached the same problem differently, adding a random energy $[-W_{dis}/2, W_{dis}/2]$ at every fifth lattice site and linearly interpolating in between in quantum calculations on a discretized lattice [109]. They concluded that the linear $R(B = 0)$ peak for the circular billiard should not be destroyed by a disorder potential with a strength chosen to match experimental conditions, with roughness in the dot wall being more crucial [14]. Ji and Berggren [25, 110] made the first investigation at the single $G(B)$ trace level (as opposed to the statistics of area distributions or averaged $R(B = 0)$ peak lineshape) for stadium-shaped billiards using a discrete lattice model [111]. Their model showed that changes in disorder potential can have a significant impact on $G(B)$ as a magnetofingerprint for the electron dynamics [110], as predicted for UCF by Feng, Lee and Stone [46], and demonstrated for diffusive quantum wires by Taylor *et al* [112] and Klepper *et al* [113].

Recently, a technique known as scanning gate microscopy (SGM) [114] has given remarkable insight into the ‘disorder potential’ and its influence on electron transport [107, 115, 116]. SGM studies of 2DEGs show significant branching of electron flow [115], and even in samples with very long mean free paths ($\ell > 10 \mu\text{m}$) significant deviations in propagation persist at scales ~ 100 nm [107]. An SGM study of a ballistic focussing structure by Aidala *et al* [116] gives a remarkable visual demonstration of the impact that small-angle scattering has on even quite short and simple ballistic transport paths between QPCs. Although

⁷ Note that other statistical measures of the fluctuations, such as the power spectrum, are also linked to fractal dimension [104].

small-angle scattering clearly doesn't prevent ballistic focussing from being observed electrically [117], it certainly forces one to question whether the concept of semiconductor billiards with long straight-line trajectories bouncing specularly off the billiard walls (see e.g., Fig. 2 of Ref. [31] or Fig. 1/6 of Ref. [5]) is a realistic picture? It also raises the question of the extent to which small-angle scattering governs the dynamics and resulting electrical properties of these devices.

Scannell *et al* [54] and See *et al* [55] have recently performed experiments aimed at illuminating the relative importance of disorder and boundary scattering in semiconductor billiards. These experiments rely on an important feature of the dopant physics of AlGaAs/GaAs heterostructures and the newly developed capability to make billiards where the 2DEG is populated electrostatically using a gate enabling the dopants to be removed [118] and the effect of small-angle dopant scattering on transport to be clearly observed. Si dopants in modulation-doped $\text{Al}_x\text{Ga}_{1-x}\text{As}/\text{GaAs}$ heterostructures with $x > 0.22$ can take one of two possible configurations [119, 120]. The first is as a shallow hydrogenic donor with a positive or neutral charge (d^+/d^0) sitting at a substitutional site. The second, known as a DX center, involves a lattice distortion that pulls the Si donor into an interstitial position along the $\langle 111 \rangle$ direction, producing a deep trap. At temperatures below ~ 150 K, the DX centers normally bind two electrons and have a negative charge (DX^-), but can be excited thermally or optically to detrap into DX^0 and DX^+ states. As described earlier, the ionized dopants impose a 'disorder potential' on the 2DEG [106], with a density of scattering sites $N = N(d^+) + N(\text{DX}^-) + N(\text{DX}^+)$, where $N(\dots)$ is the density of a particular dopant configuration. While N is normally fixed for a given heterostructure and gate-voltage configuration during cooldown [120], the allocation of particular Si site as d or DX varies each cooldown. Thus the resulting disorder potential is fixed for a single cooldown, leading to the repeatability of $G(B)$ traces shown in Fig. 3(b) and Ref. [26]. In contrast, the disorder potential should change markedly on separate cooldowns, and this would produce one of two results. If the transport in the billiard is truly ballistic, such that the disorder is negligible and the electron trajectories are determined only by scattering from the boundaries,

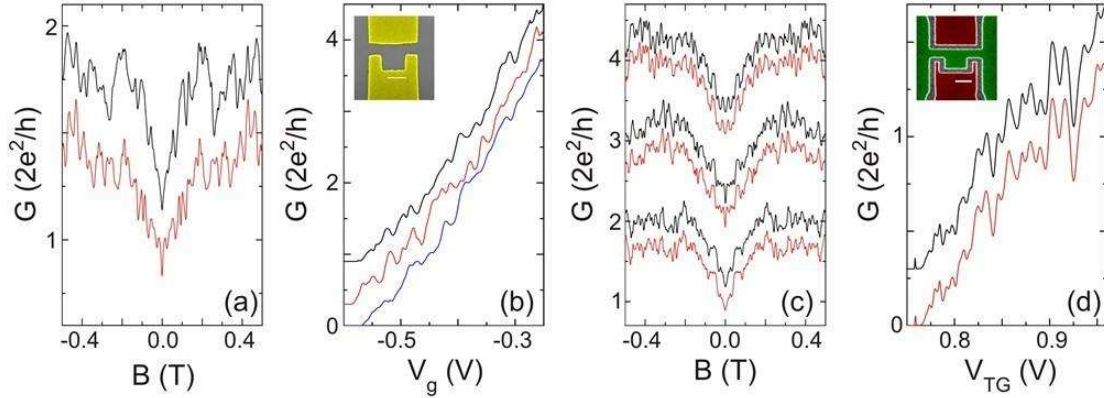


Fig. 5 Conductance G versus magnetic field B and gate voltage V from (a/b) a modulation-doped billiard and (c/d) an undoped billiard. False colour scanning electron micrographs of these devices are shown inset to (b) and (d) respectively. The scale bars indicate 500 nm. The two devices have $\ell = 2.7$ and $2.1 \mu\text{m}$ respectively. In (b), the gate bias V_g is applied to both metal gates (yellow). In (d), the gate bias V_{TG} is applied to the n^+ -GaAs top-gate (green), with the side-gates (red) grounded. In both cases $B = 0$. The traces in (a) were obtained at $V_g = -430$ (top) and -451 mV (bottom); these voltages were chosen to match $G(B = 0)$ before and after cycling. $G(B)$ traces obtained with common V_g do not match either (see Ref. [55]). The three pairs of traces in (c) were obtained at $V_{TG} = +955$ (top), $+945$ (middle) and $+935$ mV (bottom). The traces are shown in each case from top down: first (black), second (red) and third (blue) cooldown. Traces are vertically offset for clarity by: (a) bottom trace -0.3 ; (b) top trace $+0.9$, middle trace $+0.3$; (c) from bottom by $-0.3, 0, +0.7, +1.0, +1.7, +2.0$; (d) top trace $+0.3$; all in units of $2e^2/h$.

then $G(B)$ should remain the same in subsequent cooldowns (providing $T > 150$ K in between). Alternatively, if the disorder potential does affect transport, then we should see some level of change in $G(B)$, as predicted by Feng, Lee and Stone [46].

Figure 5(a) shows $G(B)$ traces obtained on separate cooldowns of the modulation-doped device inset to Fig. 5(b). There is clearly a striking difference between the traces indicative of the disorder potential affecting the transport. The gate voltage was adjusted slightly on the second cooldown in order to match $G(B = 0)$ and obtain similar injection conditions [43, 44], but See *et al* observe the same behaviour if V_g is kept the same, or takes other values as part of an extensive search for matching $G(B)$ traces [55]. As Fig. 5(b) shows, the change in disorder potential upon thermal cycling also alters the gate characteristics; the fluctuations there also originate from quantum interference [66]. This thermally-induced irreproducibility is also evident in a parallel study by Scannell *et al* [54], where the device is cooled to 300 mK and $G(B)$ is measured, the temperature is raised to an intermediate temperature T_1 for 30 minutes and returned to 300 mK, $G(B)$ is measured again, the temperature is raised to $T_2 > T_1$, re-cooled and measured again, and so on until $T_n = 298$ K. The various post-cycling $G(B)$ traces are compared to the first cooldown $G(B)$ trace using a cross-correlation analysis [121], with a precipitous drop in the correlation coefficient F from 1 to 0 obtained at $T \sim 100 - 175$ K for AlGaAs/GaAs and GaInAs/InP billiards and GaAs quantum wires. This temperature dependence points strongly to ionized dopant scattering playing a major role in influencing transport in these devices.

The ‘acid test’ for the hypothesis that the disorder potential dominates transport is to remove the dopants entirely. This requires a complete redesign of the device; a metallic gate needs to be added and this needs to overlap the contacts to the 2DEG to ensure electrical continuity. This is achieved using a degenerately-doped GaAs cap layer as the gate, which enables self-alignment of the gate to the contacts [118, 122]. The n^+ -GaAs cap is divided into three gates by shallow wet etching as shown inset to Fig. 5(d); the central gate (green) is biased positively to V_{TG} to electrostatically populate the 2DEG, the side-gates (red) can be used to tune the device further, but remain grounded here. Figure 5(c) shows $G(B)$ before and after thermal cycling to 300 K for three different V_{TG} , in each case the MCF are reproducible with high fidelity. As Fig. 5(d) shows, the gate characteristics are also highly reproducible.

Given the MCF’s role as a ‘magnetofingerprint’ [46] of electron transport within the dot, Fig. 5 demonstrates that the disorder potential has a significant, perhaps even dominant, influence on the electron dynamics. We now discuss an explanation for how and why this occurs, the implications regarding past results, and some thoughts on follow-up experiments to further elucidate the role that disorder plays in billiards.

5 Discussion

Historically, a major focus in mesoscopic physics has been to improve the mobility to access new physical regimes that are otherwise obscured by disorder. This was a key driver for work on the fractional quantum Hall effect [123, 124] and ballistic transport devices (e.g., quantum wires, dots and billiards.) as per Figs. 2(a-c). It is vital to note that the mobility, and by association ℓ , are only part of the picture. The mobility is a measure of momentum decay and it contains a weighting term $1 - \cos \theta$ [37], where θ is the scattering angle, that makes it preferentially sensitive to large-angle scattering events [37, 105, 107] Figures 2(d/e) present a more refined picture for the diffusive and ballistic regimes; here large-angle scattering sites are black and small-angle scattering sites are grey (darker shades represent a propensity towards larger scattering angles). The two pictures of diffusive transport (a/d) are essentially the same, and in either case, it is impurity scattering that dominates over boundary scattering. The two pictures for ballistic transport (b/e) are very different; as in §4.2 the ionized dopants present as small-angle scatterers with a scattering length set by the spacer thickness [107], which is much smaller than L , W and ℓ . These deflect the electron trajectories between the walls as shown, suggesting a more complex picture with a less clear-cut distinction between the traditional diffusive and ballistic regimes. Bearing in mind the thermal redistribution in

dopant potential [54, 55], this explains why the MCF changes so much between cool-downs and differs when studying the same geometry on two separate chips (see Fig. 3 of Ref. [13]).

From this perspective, the MCF in modulation-doped billiards is probably best viewed as analogous to UCF in metal films and narrow MOSFETs [47–53]. In both cases the transport is dominated by disorder scattering, the fluctuations are reproducible in a single sample/disorder configuration but vary between samples and disorder configurations, are quenched by an increase in temperature, and have certain universal statistical properties independent of the sample shape and precise dopant configuration [47] – for the UCF this is the amplitude δG which depends on the ratio of length L to coherence length L_ϕ [53], whilst for MCF in billiards, this appears to be the fractal dimension D_F which depends on a more complex combination of area A and quantum lifetime τ_q , at fixed temperature [85]. The billiard walls should help rather than hinder this analogy; their action is to repeatedly feed the electron back into the diffusive environment inside the billiard [101]. In a sense, the walls impose reflective periodic boundary conditions, effectively converting the billiard into a larger area, diffusive 2D system. The natural correlations between these mirrored sub-units, combined with the two QPCs acting as points of focus for the interference contribution may explain the loss of amplitude universality, and its replacement by the more complex universality in Fig. 4(b) [85, 89, 101]. Modeling a small-area, small-angle diffusive system with reflective boundary conditions on the edge for all but two points where trajectories can enter/exit and contribute to $G(B)$, and comparing with traditional UCF [47] may give interesting insights. Alternatively, it may be interesting to consider existing UCF models, but with the uniform random disorder replaced by repeating small ‘tiles’ of a common disorder configuration.

Nonetheless, ‘ballistic’ transport, where the walls rather than disorder is the shaping force for a given trajectory, cannot be neglected entirely in billiards. Comparing Figs. 2(b,c,e) it is clear that the diffusive effect of small-angle scattering should increase with trajectory length. As a result, the long trajectories crucial to discriminating between chaotic and regular geometries in semiclassical theories [29, 30] are likely destroyed by disorder such that all billiards are essentially chaotic, irrespective of geometry, from the perspective of the tails in the trajectory area distributions $N(\theta)$. As such, the disorder has the same ‘chaos-inducing’ effect as a Sinai diffuser [6, 61, 100], but with a scale and quantity more similar to antidot arrays [125, 126] where chaotic transport, weak localization and quantum interference fluctuations are also observed. Shorter trajectories may well survive, and we see two separate categories of these. The first are skipping orbits as highlighted by Christensson *et al* [127], and used for studying phase-breaking in dots by Bird *et al* [86–88]. These are likely protected from disorder scattering by the short distance between bounces combined with a field-induced curvature mechanism similar to that involved in the quantum Hall effect [128]. The feasibility of the survival of skipping orbits amidst the disorder potential is evident in the SGM studies by Aidala *et al* [116]. The survival of short ballistic trajectories may also explain measurements of the symmetry of MCF in the non-linear voltage regime as a function of the symmetry of billiard shape [129, 130]. Combined, the work above provides strong evidence that billiard shape is still exerts an influence on the MCF.

The second category is periodic orbits, the classic example being the diamond scar in square dots [43, 44]; this also clearly survives small-angle scattering as observed in SGM studies by Burke *et al* [68], but scars with other shapes have also been reported very recently [69]. It is easy to consider this as a straightforward case of wavefunction scarring [4, 44, 64], but there may be more to it. The diffusive effect of disorder should not only affect the unstable periodic orbit underlying the wavefunction scar, but it will do so differently between devices, between different cooldowns of the same device, and possibly also as parameters such as the gate voltage are changed. The latter may partially explain the observation of some but not all of the expected scar states in previous experiments on modulation-doped dots [66]. Wavefunction scarring in dots has recently been linked to a theory known as ‘Quantum Darwinism’ [131], where preferred states within the dot survive coupling with the environment, which acts as the ‘selection pressure’ in the theory [132]. From an experimental perspective [66], it may be that disorder presents an additional selection pressure, acting in partnership with environmental coupling, that eliminates scar states connected to much more complex underlying periodic orbits. From this perspective, it would be interesting to extend recent SGM studies of dots [68, 69] to undoped heterostructure system to see if a

greater variety of scars are observed. It would also be interesting to perform SGM studies of undoped 2DEGs and ballistic focussing structures more generally to establish the level of improvement provided by eliminating the ionized dopants. The current architecture, with a gate above the 2DEG, is unsuitable for SGM; an alternative would be to use an inverted structure [133, 134], possibly using deep etching instead of surface gates and/or patterning of the doped gate layer using focussed ion-beam lithography, as in the bilayer billiard [99].

We conclude by attempting to ‘close the loop’ and reconsider ballistic microstructures as devices for studying dynamical chaos in the quantum limit. The data in Fig. 5(c/d) shows that removal of the modulation doping instils thermal robustness in the MCF obtained from the device. Correspondingly, one would expect a significant reduction in small-angle scattering, despite this, substantial disorder will remain. This includes background impurities, some ionizable, some not, as well as interface roughness, defects in the walls of the device, etc. We suspect that this remnant disorder will prevent perfectly identical $G(B)$ from being obtained in separate undoped devices with nominally identical geometry, obviating the truly ballistic quantum dots envisioned theoretically [29–31]. One path forward might be the approach used by Chang *et al* [14], where a 6×8 array of nominally identical dots was studied to average out the MCF. This averaging of the MCF essentially constitutes an averaging of the dot disorder potentials to expose the effect of the common lithographic geometry. Attempting this using arrays of undoped dots in clean heterostructures with low background impurity densities may bring these devices close to a true ‘ballistic’ limit in terms of semiclassical dynamics, providing of course that the lithography defining their walls can be made sufficiently identical. This would be a useful challenge for future work.

Ultimately, while single quantum dots are not sufficiently ‘ballistic’ for use in studies of quantum chaos in our opinion, they have been shown to be sufficiently ballistic for potential applications [135] as ballistic rectifiers [136] and Y-branch switches [137]. The reduced small-angle scattering in undoped quantum dots offers much potential in this regard, their thermal robustness suggests they may also offer a path to devices with significantly reduced charge noise, which is a well known effect of fluctuations in the charge state of ionized dopants [138].

6 Acknowledgements

We thank the following for helpful discussions, contributions and support to this research over many years: M. Aagesen, R. Akis, N. Aoki, Y. Aoyagi, V. Bayot, J.P. Bird, S. Bollaert, S.A. Brown, A.M. Burke, A. Cappy, J. Cooper, A.G. Davies, C.P. Dettmann, L. Eaves, S. Faniel, M.S. Fairbanks, I. Farrer, D.K. Ferry, T.M. Fromhold, C. Gustin, B. Hackens, K. Ishibashi, O. Klochan, P.E. Lindelof, E.H. Linfield, L.D. Macks, P.K. Morse, G.P. Morriss, R. Newbury, Y. Ochiai, S.M. Reimann, D.A. Ritchie, L. Samuelson, I. Shorubalko, T. Sugano, W.R. Tribe and X. Wallart.

References

- [1] M.C. Gutzwiller, *J. Math. Phys.* **12**, 343 (1971).
- [2] M.V. Berry and M. Tabor, *Proc. Roy. Soc. Lond. A* **349**, 101 (1976).
- [3] S.W. McDonald and A.N. Kaufman, *Phys. Rev. Lett.* **42**, 1189 (1979).
- [4] E.J. Heller, *Phys. Rev. Lett.* **53**, 1515 (1984).
- [5] E.J. Heller and S. Tomsovic, *Physics Today* **46(7)**, 38 (1993).
- [6] Ya. G. Sinai, *Russ. Math. Survey* **25**, 137 (1970).
- [7] M.C. Gutzwiller, *Chaos in Classical and Quantum Mechanics* (Springer-Verlag, New York, 1990).
- [8] H.-J. Stöckmann, *Quantum Chaos: An Introduction* (Cambridge University Press, Cambridge, 1999).
- [9] H.-J. Stöckmann and J. Stein, *Phys. Rev. Lett.* **64**, 2215 (1990).
- [10] S. Sridhar, *Phys. Rev. Lett.* **67**, 785 (1991).
- [11] J. Stein, *Phys. Rev. Lett.* **68**, 2867 (1992).
- [12] H.-D. Gräf *et al*, *Phys. Rev. Lett.* **69**, 1296 (1992).
- [13] C.M. Marcus, A.J. Rimberg, R.M. Westervelt, P.F. Hopkins and A.C. Gossard, *Phys. Rev. Lett.* **69**, 506 (1992).
- [14] A.M. Chang, H.U. Baranger, L.N. Pfeiffer and K.W. West, *Phys. Rev. Lett.* **73**, 2111 (1994).

- [15] M.J. Berry, J.A. Katine, R.M. Westervelt and A.C. Gossard, *Phys. Rev. B* **50**, 17721 (1994).
- [16] M.F. Crommie, C.P. Lutz and D.M. Eigler, *Science* **262**, 218 (1994).
- [17] E.J. Heller, M.F. Crommie, C.P. Lutz and D.M. Eigler, *Nature* **369**, 464 (1994).
- [18] C. Ellegaard *et al*, *Phys. Rev. Lett.* **75**, 1546 (1995).
- [19] K. Schaadt, A.P.B. Tufaile and C. Ellegaard, *Phys. Rev. E* **67**, 026213 (2003).
- [20] V. Milner, J.L. Hansen, W.C. Campbell and M.G. Raizen, *Phys. Rev. Lett.* **86**, 1514 (2001).
- [21] N. Friedman, A. Kaplan, D. Carasso and N. Davidson, *Phys. Rev. Lett.* **86**, 1518 (2001).
- [22] C. Gmachl *et al*, *Science* **280**, 1556 (1998).
- [23] V. Doya, O. Legrand and F. Mortessagne, *Opt. Lett.* **26**, 872 (2001).
- [24] V. Doya, O. Legrand, F. Mortessagne and C. Miniatura, *Phys. Rev. Lett.* **88**, 014102 (2002).
- [25] K.-F. Berggren and Z.-L. Ji, *Chaos* **6**, 543 (1996).
- [26] C.M. Marcus, R.M. Westervelt, P.F. Hopkins and A.C. Gossard, *Chaos* **3** 643 (1993).
- [27] W.A. Lin, J.B. Delos and R.V. Jensen, *Chaos* **3**, 655 (1993).
- [28] M. Prusty and H. Schanz, *Phys. Rev. Lett.* **96**, 130601 (2006).
- [29] R.A. Jalabert, H.U. Baranger and A.D. Stone, *Phys. Rev. Lett.* **65**, 2442 (1990).
- [30] H.U. Baranger, R.A. Jalabert and A.D. Stone, *Phys. Rev. Lett.* **70**, 3876 (1993).
- [31] R.V. Jensen, *Nature* **373**, 16 (1995).
- [32] R. Dingle, H.L. Störmer, A.C. Gossard and W. Wiegmann, *Appl. Phys. Lett.* **33**, 665 (1978).
- [33] A.Y. Cho, *Appl. Phys. Lett.* **19**, 467 (1971).
- [34] T.J. Thornton, M. Pepper, H. Ahmed, D. Andrews and G.J. Davies, *Phys. Rev. Lett.* **56**, 1198 (1986).
- [35] R.P. Taylor, *Nanotechnology* **5**, 183 (1994).
- [36] C.W.J. Beenakker and H. van Houten, *Solid State Physics* **44**, 1 (1991).
- [37] P.T. Coleridge, *Phys. Rev. B* **44**, 3793 (1991).
- [38] Y. Aharonov and D. Bohm, *Phys. Rev.* **115**, 485 (1959).
- [39] R.G. Chambers, *Phys. Rev. Lett.* **5**, 3 (1960).
- [40] A. Tonomura *et al*, *Phys. Rev. Lett.* **56**, 792 (1986).
- [41] R.A. Webb, S. Washburn, C.P. Umbach and R.B. Laibowitz, *Phys. Rev. Lett.* **54**, 2696 (1985).
- [42] G. Timp *et al*, *Phys. Rev. Lett.* **58**, 2814 (1987).
- [43] J.P. Bird *et al*, *Chaos, Solitons and Fractals* **8**, 1299 (1997).
- [44] R. Akis, D.K. Ferry and J.P. Bird, *Jap. J. Appl. Phys.* **36**, 3981 (1997).
- [45] R.P. Taylor *et al*, *Surf. Sci.* **196**, 52 (1988).
- [46] S. Feng, P.A. Lee and A.D. Stone, *Phys. Rev. Lett.* **56**, 1960 (1986).
- [47] P.A. Lee, A.D. Stone and H. Fukuyama, *Phys. Rev. B* **35**, 1039 (1987).
- [48] P.A. Lee and A.D. Stone, *Phys. Rev. Lett.* **55**, 1622 (1985).
- [49] B.L. Altshuler, *JETP Lett.* **41**, 648 (1985).
- [50] J.C. Licini, D.J. Bishop, M.A. Kastner and J. Melngailis, *Phys. Rev. Lett.* **55**, 2987 (1985).
- [51] S.B. Kaplan and A. Hartstein, *Phys. Rev. Lett.* **56**, 2403 (1986).
- [52] W.J. Skocpol *et al*, *Phys. Rev. Lett.* **56**, 2865 (1986).
- [53] W.J. Skocpol, *Phys. Scr.* **T19**, 95 (1987).
- [54] B.C. Scannell *et al*, *arXiv:1106.5823* (2011).
- [55] A.M. See *et al*, *In press for Phys. Rev. Lett.*; *ArXiv* 1204.0158 (2012).
- [56] C.W.J. Beenakker and H. van Houten, *Phys. Rev. Lett.* **63**, 1857 (1989).
- [57] C.J.B. Ford, S. Washburn, M. Büttiker, C.M. Knoedler and J.M. Hong, *Phys. Rev. Lett.* **62**, 2724 (1989).
- [58] A.M. Chang, T.Y. Chang and H.U. Baranger, *Phys. Rev. Lett.* **63**, 996 (1989).
- [59] T. Tél, *Phys. Rev. A* **36**, 1502 (1987).
- [60] R. Blümel and U. Smilansky, *Phys. Rev. Lett.* **64**, 241 (1990).
- [61] E. Doron, U. Smilansky and A. Frenkel, *Phys. Rev. Lett.* **65**, 3072 (1990).
- [62] R.B.S. Oakeshott and A. MacKinnon, *Superlatt. Microstruct.* **11**, 145 (1992).
- [63] K. Nakamura and H. Ishio, *J. Phys. Soc. Jpn* **61**, 3939 (1992).
- [64] P.B. Wilkinson, T.M. Fromhold, L. Eaves, F.W. Sheard, N. Miura and T. Takamasu, *Nature* **380**, 608 (1996).
- [65] R. Akis, D.K. Ferry and J.P. Bird, *Phys. Rev. Lett.* **79**, 123 (1997).
- [66] J.P. Bird *et al*, *Phys. Rev. Lett.* **82**, 4691 (1999).
- [67] R. Crook, C.G. Smith, A.C. Graham, I. Farrer, H.E. Beere and D.A. Ritchie, *Phys. Rev. Lett.* **91**, 246803 (2003).
- [68] A.M. Burke, R. Akis, T.E. Day, G. Speyer, D.K. Ferry and B.R. Bennett, *Phys. Rev. Lett.* **104**, 176801 (2010).
- [69] N. Aoki *et al*, *In press for Phys. Rev. Lett.* (2012).
- [70] G. Bergmann, *Phys. Rep.* **107**, 1 (1984).
- [71] R. Akis, D.K. Ferry, J.P. Bird and D. Vasileska, *Phys. Rev. B* **60**, 2680 (1999).
- [72] R. Akis, D. Vasileska, D.K. Ferry and J.P. Bird, *J. Phys.: Condens. Matter* **11**, 4657 (1999).
- [73] J.P. Bird, R. Akis and D.K. Ferry, *Phys. Rev. B* **60**, 13676 (1999).
- [74] H.U. Baranger, R.A. Jalabert and A.D. Stone, *Chaos* **3**, 665 (1993).

- [75] I.H. Chan, R.M. Clarke, C.M. Marcus, K. Campman and A.C. Gossard, Phys. Rev. Lett. **74**, 3876 (1995).
- [76] C.M. Marcus, Private Communication.
- [77] J.P. Bird *et al*, Phys. Rev. B **52**, 14336 (1995).
- [78] M.W. Keller *et al*, Phys. Rev. B **53**, 1693 (1996).
- [79] S.E. Laux, D.J. Frank and F. Stern, Surf. Sci. **196**, 101 (1988).
- [80] A. Kumar, S.E. Laux and F. Stern, Phys. Rev. B **42**, 5166 (1990).
- [81] R. Ketzmerick, Phys. Rev. B **54**, 10841 (1996).
- [82] A.P. Micolich *et al*, J. Phys.: Condens. Matter **10**, 1339 (1998).
- [83] A.S. Sachrajda *et al*, Phys. Rev. Lett. **80**, 1948 (1998).
- [84] R.P. Taylor *et al*, Phys. Rev. Lett. **78**, 1952 (1997).
- [85] A.P. Micolich *et al*, Phys. Rev. Lett. **87**, 036802 (2001).
- [86] J.P. Bird *et al*, Surf. Sci. **361/362**, 730 (1996).
- [87] J.P. Bird *et al*, Phys. Stat. Sol. (b) **204**, 314 (1997).
- [88] J.P. Bird *et al*, J. Phys.: Condens. Matter **10**, L55 (1998).
- [89] A.P. Micolich *et al*, Phys. Rev. B **70**, 085302 (2004).
- [90] A. Budiyo and K. Nakamura, Chaos, Solitons and Fractals **17**, 89 (2003).
- [91] R.P. Taylor *et al*, Phys. Rev. B **58**, 11107 (1998).
- [92] A.P. Micolich, R.P. Taylor, R. Newbury, T.M. Fromhold and C.R. Tench, Europhys. Lett. **49**, 417 (2000).
- [93] H. Hennig, R. Fleischmann, L. Hufnagel and T. Geisel, Phys. Rev. E **76**, 015202 (2007).
- [94] Y. Takagaki and K.H. Ploog, Phys. Rev. B **61**, 4457 (2000).
- [95] E. Louis and J.A. Vergés, Phys. Rev. B **61**, 13014 (2000).
- [96] G. Benenti, G. Casati, I. Guarneri and M. Terraneo, Phys. Rev. Lett. **87**, 014101 (2001).
- [97] F.A. Pinheiro and C.H. Lewenkopf, Braz. J. Phys. **36**, 379 (2006).
- [98] I. Guarneri and M. Terraneo, Phys. Rev. E **65**, 015203 (2001).
- [99] A.P. Micolich *et al*, Appl. Phys. Lett. **80**, 4381, (2002).
- [100] T.M. Fromhold, C.R. Tench, R.P. Taylor, A.P. Micolich and R. Newbury, Physica B **249-251**, 334 (1998).
- [101] C.A. Marlow *et al*, Phys. Rev. B **73**, 195318 (2006).
- [102] T.P. Martin *et al*, Superlatt. Microstruct. **34**, 179 (2003); Phys. Rev. B **77**, 155309 (2008).
- [103] H. Hegger *et al*, Phys. Rev. Lett. **77**, 3885 (1996).
- [104] H.-O. Peitgen and D. Saupe (eds.), *The Science of Fractal Images* (Springer-Verlag, New York, 1988).
- [105] S.J. MacLeod *et al*, Phys. Rev. B **80**, 035310 (2009).
- [106] J.A. Nixon and J.H. Davies, Phys. Rev. B **41**, 7929 (1990).
- [107] M.P. Jura *et al*, Nature Physics **3**, 841 (2007).
- [108] J.A. Nixon, J.H. Davies and H.U. Baranger, Phys. Rev. B **43**, 12638 (1991).
- [109] H.U. Baranger, Phys. Rev. B **42**, 11479 (1990).
- [110] Z.-L. Ji and K.-F. Berggren, Phys. Rev. B **52**, 11607 (1995).
- [111] Y. Wang, J. Wang and H. Guo, Phys. Rev. B **49**, 1928 (1994).
- [112] R.P. Taylor *et al*, Inst. Phys. Polish Acad. Sci. **1**, 83 (1988); Can. J. Phys. **70**, 979 (1992).
- [113] S.J. Klepper, O. Millo, M.W. Keller, D.E. Prober and R.N. Sacks, Phys. Rev. B **44**, 8380 (1991).
- [114] M.A. Eriksson *et al*, Appl. Phys. Lett. **69**, 671 (1996).
- [115] M.A. Topinka *et al*, Nature **410**, 183 (2001).
- [116] K.E. Aidala *et al*, Nature Physics **3**, 464 (2007).
- [117] H. van Houten *et al*, Phys. Rev. B **39**, 8556 (1989).
- [118] A.M. See *et al*, Appl. Phys. Lett. **96**, 112104 (2010).
- [119] A.R. Long, J.H. Davies, M. Kinsler, S. Vallis and M.C. Holland, Semicond. Sci. Technol. **8**, 1581 (1993).
- [120] E. Buks, M. Heiblum and H. Shtrikmann, Phys. Rev. B **49**, 14790 (1994).
- [121] R.P. Taylor, A.P. Micolich, R. Newbury, T.M. Fromhold, Phys. Rev. B **56**, 12733 (1997).
- [122] B.E. Kane, L.N. Pfeiffer, K.W. West and C.K. Harnett, Appl. Phys. Lett. **63**, 2132 (1993).
- [123] H.L. Störmer, Rev. Mod. Phys. **71**, 875 (1999).
- [124] W. Pan *et al*, Phys. Rev. Lett. **106**, 206806 (2011).
- [125] O. Yevtushenko, G. Lütjering, D. Weiss and K. Richter, Phys. Rev. Lett. **84**, 842 (2000).
- [126] A. Dorn, E. Bieri, T. Ihn, K. Ensslin, D.D. Driscoll and A.C. Gossard, Phys. Rev. B **71**, 035343 (2005).
- [127] L. Christensson *et al*, Phys. Rev. B **57**, 12306 (1998).
- [128] M. Büttiker, Phys. Rev. B **38**, 9375 (1988).
- [129] A. Löfgren *et al*, Phys. Rev. Lett. **92**, 046803 (2004).
- [130] C.A. Marlow, R.P. Taylor, M. Fairbanks, I. Shorubalko and H. Linke, Phys. Rev. Lett. **96**, 116801 (2006).
- [131] W.H. Zurek, Nature Physics **5**, 181 (2009).
- [132] R. Brunner, R. Akis, D.K. Ferry, F. Kuchar and R. Meisels, Phys. Rev. Lett. **101**, 024102 (2008).
- [133] U. Meirav, M. Heiblum and F. Stern, Appl. Phys. Lett. **52**, 1268 (1988).
- [134] U. Meirav, M.A. Kastner and S.J. Wind, Phys. Rev. Lett. **65**, 771 (1990).
- [135] S.M. Goodnick and J.P. Bird, IEEE Trans. Nanotech. **2**, 368 (2003).
- [136] A.M. Song *et al*, Appl. Phys. Lett. **79**, 1357 (2001).
- [137] L. Worschech, H.Q. Xu, A. Forchel and L. Samuelson, Appl. Phys. Lett. **79** 3287 (2001).
- [138] C. Buizert *et al*, Phys. Rev. Lett. **101**, 226603 (2008).